Eur. Phys. J. Spec. Top. (2025) 234:5009–5019
https://doi.org/10.1140/epjs/s11734-025-01501-6

THE EUROPEAN PHYSICAL JOURNAL SPECIAL TOPICS

Review

Cosmic ray sources and detectors

Pravata Kumar Mohanty[a]

Department of High Energy Physics, Tata Institute of Fundamental Research, Homi Bhabha Road, Mumbai, Maharashtra 400005, India

Received 7 October 2024 / Accepted 29 January 2025 / Published online 24 February 2025

Abstract The origin of cosmic rays has remained an enduring mystery in astrophysics since their discovery by Victor Hess in 1912. However, extensive studies on the energy spectrum, mass composition, and angular distributions of cosmic rays have been conducted through both space-based and ground-based experiments. Although space-based experiments are limited to measuring cosmic rays with energies below about 10^{14} eV, their high precision has led to the discovery of several new features in the cosmic ray spectrum. However, ground-based detector arrays have provided valuable insights into cosmic rays at higher energies, offering new information on their spectrum, composition, and angular distributions. This paper reviews the major cosmic ray detectors currently in operation, both in space and on the ground, followed by an in-depth look at the GRAPES-3 experiment, which operates in Ooty, India, and focuses on the TeV-PeV energy range. Recent findings from GRAPES-3 on the cosmic ray spectrum and anisotropy are discussed, along with an update on the ongoing upgrade of the experiment.

1 Introduction

Cosmic rays are the most energetic form of radiation found in nature. They consist of high-energy charged particles, primarily atomic nuclei, traveling at relativistic speeds. Most cosmic rays are composed of hydrogen nuclei, or protons (90%), and helium nuclei (9%), with the remaining 1% consisting of heavier elements, such as carbon, nitrogen, oxygen, silicon, aluminum, iron, and others. This composition mirrors that of the solar system with some variations, indicating a stellar origin. Cosmic rays offer a broad representation of the periodic table [1].

Cosmic rays enter our solar system from the interstellar medium. Due to the higher magnetic field of the heliosphere compared to the interstellar medium, low-energy cosmic rays, specifically those below 100 GeV, are influenced by the heliospheric magnetic field, resulting in modulations that provide information about solar activity and space weather [2]. Earth's magnetosphere serves as a shield for low-energy cosmic rays. However, cosmic rays more easily penetrate the Earth's atmosphere through the polar regions.

The energy of cosmic rays spans a vast range, from 10^8 eV to 10^{20} eV. For comparison, visible light has an energy around 1 eV, X-rays are approximately 10^3 eV, and emissions from radioactive decay, such as alpha, beta, and gamma rays, are in the range of 10^6 eV. Particles such as electrons and protons in the solar corona, where the temperature is around 1 million degrees, have an average energy of about 10^2 eV. The energy density of cosmic rays is roughly 1 eV per cubic centimeter, comparable to that of magnetic fields, starlight, and the cosmic microwave background radiation in the universe.

2 Cosmic ray sources

Cosmic rays were discovered more than 100 years ago. However, the problem of their origin is still to be resolved. The challenge arises, because cosmic rays are charged particles. Hence, the interstellar magnetic field deflects their trajectories from their original path, making their distribution almost isotropic (similar intensity in different

[a] e-mail: pkm@tifr.res.in (corresponding author)

directions). Thus, when cosmic rays are observed on Earth, their trajectories cannot be traced back to their sources. However, measurements of their mass composition suggest that they originate from stellar sources.

Supernova remnants (SNRs) are widely considered the most likely source of cosmic rays at energies between a few hundreds of MeV and a few PeV (10^{15} eV). The idea was first proposed by Bade and Zwicky who hypothesized that SNRs could accelerate cosmic rays [3], and later supported by Ginzburg and Syrovatskii [4] follow the fact that the cosmic ray energy density is $\rho_{CR} \sim$1 eV$/cm^3$. The galactic disk thickness is about 200 pc, and the radius is roughly 15 kpc. This suggests that to fill the entire volume of the Galaxy ($V_G = 4 \times 10^{66}\, cm^3$) with CRs having an escape time of $\tau_{esc} \sim 6 \times 10^6\, yrs$, the total power required would be $P_{CR} = V_G \rho_{CR}/\tau_{esc} = 5 \times 10^{40}\, erg/s$.

In a supernova explosion around ten times, the mass of the Sun is ejected with a velocity of $v \sim 5 \times 10^8\, cm/s$. The frequency of SN explosion rate in our galaxy is assumed to be about one in 30 years. By calculating the power from the rate of kinetic energy released per year, we obtain $P_{SN} = 3 \times 10^{42}\, erg/s$. If we consider lower efficiencies ($\sim 10^{-2}$) due to energy losses and other factors, we can conclude that SNs provide sufficient power to account for the observed cosmic ray density.

It is believed that the low-energy charged particles are repeatedly encountered by the shocks of the supernova explosion while gaining energy in each encounter. Cosmic ray interactions in the source environment can produce neutral radiation such as gamma rays and neutrinos, which can come straight from the source to the Earth. Therefore, observation of these neutral radiation can help us to identify the sources of cosmic rays. Considerable progress has occurred in the observation of gamma rays and neutrinos during the past two decades, hinting about the sources of cosmic rays. Further observations and interpretation are required to get a precise answer on the cosmic ray origin.

3 Cosmic ray detectors

The number of cosmic ray particles hitting Earth per unit area, per unit solid angle, per unit time (called flux) decreases rapidly with increasing energy following a power-law dependence on energy (flux $\propto E^{-\gamma}$, where γ is called the spectral index and its nominal value is about 2.7 below $\sim$ 3 PeV). For example, at 10^{11} eV, about one cosmic ray passes through a square meter each second. At 10^{15} eV (PeV), the rate drops to one per square meter per year, and at 10^{18} eV (EeV), it is approximately one per square kilometer per year. Thus, detectors of varying sizes are needed for statistically significant detection of cosmic rays across this broad energy spectrum.

Cosmic ray measurements below about 10^{14} eV (100 TeV) are carried out mainly by satellite- or balloon-borne experiments. They are more accurate, because cosmic rays are detected directly before they interact in the atmosphere of the Earth. However, space-based observations are limited to below 100 TeV owing to the steeply falling rate of cosmic rays with increasing energy and the weight limits of the detectors that can be accommodated. Ground-based detector arrays complement space-based observations up to the highest energies (10^{20} eV).

Space-based detectors are mainly particle-type detectors, similar to those used in accelerator experiments. Detectors designed with large magnetic fields can differentiate between particle and antiparticle. In addition, they have elements for tracking the particle. They also contain calorimeters that measure the energy of the particle.

Ground-based detectors measure the charged particle densities in the extensive air shower (EAS) which provides the core location. The lateral density measurements are used to obtain the size representing the total number of particles and the age representing the development stage of the shower. Relative arrival times are measured to obtain the direction of the shower. Measurement of the muon density in the shower helps to obtain the mass or composition of the primary cosmic rays. It is also a sensitive observable for gamma and charged cosmic ray differentiation.

Ground-based detector arrays mainly include plastic scintillators, water Cherenkov tanks, and fluorescence telescopes. More recently, radio antenna arrays have also been proven to be effective for cosmic ray measurements beyond 10^{17} eV. Plastic scintillators measure charged particle densities in air showers by depositing a fraction of their energy in the scintillator medium, which produces scintillation light in the blue wavelength region. The water Cherenkov detectors measure the density of charged particles in the EAS through the Cherenkov light produced in the water by the passage of charged particles. Fluorescence telescopes measure the florescence light produced by the passage of charged particles by exciting nitrogen molecules in the air medium. They provide a measurement of the longitudinal profile of the EAS development. Although scitillators and water Cherenkov detectors operate all the time, fluorescence telescopes operate in the dark night, hence limited to a duty cycle of $\sim$ 10%.

3.1 Space-based cosmic ray detectors

Some of the major ongoing space-based cosmic ray detectors are described below.

The Alpha Magnetic Spectrometer (AMS-02) experiment is located on the International Space Station. Its main design goals are to (1) distinguish hadrons from leptons, (2) distinguish particle and antiparticle, and (3) provide chemical and isotopic composition information in the energy range of sub-GeV to a few TeV. It contains a permanent magnet that provides a magnetic field of 1.4 kG at its center. The magnet is surrounded by an array of particle detectors which measure the momentum and charge of the passing nuclei and particles. Transition Radiation Detector identifies electrons and positrons through Transition Radiation while rejecting protons with an efficiency of 10^3. Another function of this detector is to distinguish nuclei based on their energy loss rate (dE/dx). The system includes nine precision silicon tracker planes, consisting of 200,000 channels, to measure particle charge sign and momentum with unprecedented precision. The upper and lower time-of-flight counters are above and below the magnet to (1) provide the charged particle trigger, (2) determine the velocity and direction of the incoming particles, and (3) measure their charge using dE/dx. The Anti-Coincidence Counters are used to block cosmic rays entering from the side with a measured efficiency of 0.99999. The Ring Imaging Cherenkov detector is equipped with 10,880 photosensors which measures the charge and velocity of passing particles. The ECAL, a 3D imaging instrument made from 1,200 pounds of lead and 50,000 scintillating fibers, provides a shower measurement with 17 radiation lengths and 1,296 measuring cells. It accurately measures the energy and direction of TeV positrons and electrons, with an energy resolution of approximately 2% and an angular resolution of 0.5° for E>100 GeV. Together, the ECAL and tracker separate protons from electrons and positrons with an efficiency of 10^4 [5].

The CALorimetric Electron Telescope (CALET) is a collaborative mission involving Japan, Italy, and the United States, which has operated on the International Space Station (ISS) since its launch on August 19, 2015. Its primary goal is to measure the electrons and charged nuclei of cosmic rays to better understand the origin, acceleration, and propagation of cosmic rays. The main instrument aboard CALET is the calorimeter, which can detect gamma rays from approximately 1 GeV to several TeV, as well as protons and nuclei up to 1 PeV. In addition, CALET includes a Gamma-ray Burst Monitor, which is sensitive to photons from 7 keV to 28 MeV. The CAL consists of three major subdetectors: the CHarge Detector (CHD), the IMaging Calorimeter (IMC), and the Total AbSorption Calorimeter (TASC). The CHD is a hodoscope made up of two orthogonal layers, each containing 14 plastic scintillating paddles, which are read by photomultiplier tubes (PMTs). Measures the absolute charge of primary particles, from protons to iron nuclei, with a charge resolution of approximately 0.1−0.3 e. The IMC is a sampling calorimeter composed of pairs of crossed x–y layers of finely segmented plastic scintillating fibers, read by multi-anode PMTs. These layers are interspersed with seven tungsten sheets, which contribute most of the IMC's total thickness of approximately 3 radiation lengths. The tungsten sheets initiate and develop particle showers, whereas the scintillating fibers provide high-resolution spatial imaging, aiding in particle identification and tracking. The TASC consists of 12 crossed layers of lead tungstate (PbWO4 or PWO) logs, with a total thickness of 27 radiation lengths. The top PWO layer is read by PMTs, whereas the lower layers are equipped with photodiodes and avalanche photodiodes (PD/APDs) for readout. The calorimeter depth enables almost complete containment of electromagnetic showers produced by primary electrons and photons, with energies reaching up to tens of TeV [6].

The DArk Matter Particle Explorer (DAMPE) is a collaborative mission that involves universities and institutes from China, Switzerland, and Italy. Launched on December 17, 2015, into a Sun-synchronous orbit at an altitude of 500 km, it is still in operation. DAMPE's primary scientific goal is to measure electrons and photons with high-energy resolution and extended energy ranges, aiming to detect potential signatures of dark matter. DAMPE detects electrons and photons in the energy range of 5 GeV to 10 TeV, with an energy resolution of about 1.5% at 100 GeV. For cosmic rays, their detection range extends from 100 GeV to 100 TeV, with an energy resolution better than 40% at 800 GeV. The instrument's geometrical factor is approximately 0.3 m^2 sr for electrons and photons, and 0.2 m^2 sr for cosmic rays, with an angular resolution of 0.1° at 100 GeV. The DAMPE instrument includes a double-layer plastic scintillator detector (PSD) serving as an anticoincidence detector, followed by a Silicon–Tungsten Tracker-Converter (STK). The STK consists of six tracking double layers, each made up of two single-sided silicon strip detectors that measure two orthogonal views perpendicular to the pointing direction. Three tungsten plates, each 1 mm thick, are positioned in front of the second, third, and fourth tracking layers to facilitate photon conversion. Following the STK is an imaging calorimeter composed of 14 layers of Bismuth Germanium Oxide (BGO) bars arranged in a hodoscopic pattern, with a total thickness of about 31 radiation lengths. Beneath the calorimeter, a layer of neutron detectors is included. The combined thickness of the BGO calorimeter and STK corresponds to about 33 radiation lengths, making DAMPE's calorimeter the deepest ever used in space. Finally, a Neutron Detector (NUD) is placed below the calorimeter to detect delayed neutrons from hadron showers and enhance electron/proton separation. The NUD consists of 16 boron-doped plastic scintillator plates, each measuring 19.5×19.5 cm^2 and 1 cm thick, with readout provided by photomultipliers [7].

3.2 Ground-based cosmic ray detectors

Primary cosmic rays, when they enter the atmosphere of Earth, interact with nuclei of nitrogen or oxygen molecules. The interaction leads to the production of secondary particles. A shower is developed that includes charged and neutral particles. The multiplication of the particles occurs up to a certain depth in the atmosphere depending on the energy of the primary cosmic rays, and after that the secondary particles start to get absorbed because of the ionization losses. The particles in the shower at the observational level include mostly gammas, followed by electrons (and positrons), and muons. The muons about 210 times more massive than electrons can penetrate deeper in the atmosphere, even the higher energy muons can pass kilometers underground. Due to the time dilation effect, a major fraction of muons which are produced in the upper atmosphere could reach the ground level, because they can travel a longer distance before they decay. Neutrinos are also produced in the shower; however, they are weakly interacting particles and require large-volume detectors for their detection. Many of them can travel from one side to the other of the Earth. Particles in the shower travel nearly the speed of light as they are relativistic. They are spread over several tens of square meters or even several square kilometers on the ground. The energy of primary cosmic rays that hit the top of the atmosphere is distributed among thousands to millions of secondary particles produced in the shower. Some of the ground-based detector arrays designed to study cosmic rays through measurement of shower particles are described below.

The Tibet-AS$_\gamma$ observatory is located in Tibet (30.1°N, 90.5°E, 4,300 m a.s.l.) with an atmospheric overburden of 600 g cm^{-2}. It is a collaboration of institutes from China, Japan, and Italy. The experiment was designed to record both cosmic ray and gamma-ray-initiated EAS in the atmosphere in the energy range of several TeV to 100 PeV. The experiment consists of an array of 597 scintillator detectors of 0.5 m^2 area each, spread over an area of 65,700 m^2. It also contains 64 underground Cherenkov muon detectors located in four pools with 16 units per pool. The scintillator detectors observe the electromagnetic components in the EAS which provides the energy and direction measurement of the primary particle. The muon detector measures the muon component in the EAS that provides discrimination between gamma and cosmic ray primaries [8].

The Large High-Altitude Air Shower Observatory (LHAASO) is located in Mt. Haizi (29.2°N, 100.1°E, 4410 m a.s.l.), Sichuan province, China with an atmospheric depth of 600 g cm^{-2}. The experiment is designed to observe cosmic rays from sub-TeV to 100 PeV. The experiment consists of (1) 5216 electromagnetic detectors (ED) of 1 m^2 each with an inter-separation of 15 m, (2) 1188 muon detectors (MD) of 36 m^2 each, (3) a water Cherenkov detector array (WCDA) of 78000 m^2 area, and (4) 18 wide field Cherenkov telescopes (WFCTA). EDs measure secondary electromagnetic particles in the shower. The scintillation light generated by charged particles in the plastic scintillator is collected by wavelength-shift fibers, transmitted to a photomultiplier tube (PMT), and converted into electrical signals. MDs measure the muon content of the EAS. A water bag containing ultrapure water is placed in a concrete tank with a diameter of 6.8 m and a height of 1.2 m, and a PMT is installed at the top center of the water bag to collect the Cherenkov light generated in the water by muons that enter the tank. The WCDAs measure charged particles and photons in the EAS. It is made up of 3 adjacent large ponds (two with a dimension of 150 m × 150 m and one with a dimension of 300 m × 110 m), and the depth of the water is 4.5 m. The ponds are subdivided into 3120 cells in size of 5 m × 5 m, each provided with 2 PMTs to collect Cherenkov light generated in the water by charged particles in the shower. The WFCTAs measure the Cherenkov lights generated in the EAS. Each telescope consists of a reflector made of a 5 m^2 spherical aluminized mirror and a silicon photo multiplier (SiPMs) camera with 32 × 32 pixels. The field of view of a telescope is 16° ×16°, and the pixel size of the camera is 0.5° ×0.5° [9].

The High-Altitude Water Cherenkov (HAWC) Gamma-Ray Observatory is located in the Sierra Negra Volcano, Puebla, Mexico (19°N, 97°W, 4100 m above sea level). It is a collaboration of institutions from Mexico, the United States, South America, and Europe. Its energy coverage ranges from sub-TeV to 1 PeV. It consists of 300 densely packed water Cherenkov detectors (WCD). The coverage area of the array is 22,000 m^2. Each WCD tank contains 200000 ls of water and 4 PMTs. It is designed to record both gamma- and cosmic-ray-initiated showers. The energy coverage ranges from 500 GeV to several hundred TeV [10].

GRAPES-3 (Acronym for Gamma-Ray Astronomy at PeV Energies Phase-3) is an air shower experiment located in Ooty, India (11.4°N, 76.7°E, 2200 m a.s.l.). It is a collaboration of institutions and universities from India and Japan. It consists of an array of plastic scintillator detectors of 1 m^2 area each with inter-separation of 8 m. The coverage area of the array is 25,000 m^2. The second component of the experiment is a 560 m^2 tracking muon detector. The array records EAS over an energy range of 10 TeV to 10 PeV. A more detailed description of the experiment is given in the later section [11, 12].

The KASCADE experiment located in Karlsruhe, Germany was designed to study cosmic rays in the PeV energies, which operated until 2008. It is located almost at sea level (110 m above sea level) on the Karlsruhe Institute of Technology campus. It contains 252 scintillation detector stations with a 13 m spacing spread over an area of

40,000 m^2. The scintillator detector was designed to measure both electromagnetic and muon density simultaneously. The array is sensitive to the measurement of cosmic rays above 100 TeV to 100 PeV [13]. The KASCADE-Grande is the enlargement of the KASCADE array to extend the energy range to 10^{18} eV. It deployed a sparse array 37 scintillator detector stations of 10 m^2 area each with a total coverage area of 700×700 m^2. These detectors provide the measurement of all charged particles in the EAS [14].

IceTop is the surface component of the IceCube Neutrino Observatory at the South Pole. It is designed for cosmic ray observations from sub-PeV to over 1 EeV. The IceTop array, at an altitude of 2835 m above sea level, consists of 162 tanks filled with clear ice distributed in 81 stations spread over an area of 1 km^2. Each station has two tanks separated by 10 m. Having two tanks in a station allows for the selection of a subset of events in which both tanks have signal above threshold, suppressing the background of small showers hitting only one tank. The stations are arranged on a triangular grid with a typical spacing of 125 m. In addition, IceTop has a dense infill array where the distance between stations is significantly smaller [15].

The Pierre Auger Observatory (PAO) is located in the province of Mendoza, Argentina (69.2°W, 35.2°S, 1400 m). The observatory consists of 1660 water Cherenkov particle detector stations, deployed on a 1.5 km triangular grid, covering an effective area of 3,000 km^2 along with four stations, each containing six air fluorescence telescopes used to detect emitted fluorescence light in the shower. While surface detectors provide measurements of shower core location, direction, and shower size, fluorescence telescopes provide the measurement of the shower depth maximum, which is used for the measurement of cosmic ray mass composition. The observatory has been operating since 2008. It has measured cosmic ray spectrum and composition over an energy range of 10^{17} to 10^{20} eV. It has confirmed the existence of the GZK cutoff [16].

The Telescope Array (TA) experiment is located in Utah, United States (112.9° W, 39.3° N, 1370 m above sea level). It is a collaboration between universities and institutions in the United States, Japan, Korea, Russia, and Belgium. It consists of a surface detector array with 507 stations arranged in a square grid. Each detector has two 3 m^2 layers of plastic scintillators that detect charged EAS particles. The stations are spaced by 1.2 km, giving a total effective area of 700 km^2. The sky over the surface detectors is viewed by fluorescence detectors, which directly measure photons produced by the propagation of an EAS through the atmosphere, providing a calorimetric measurement of the shower energy. The mass of the primary cosmic ray is estimated using the fluorescence detectors by determining the shower depth maximum. TA has a energy coverage similar to PAO and it has also observed the GZK cutoff from the Northern hemisphere [17].

4 Cosmic ray measurements

4.1 Cosmic ray composition and energy spectrum

Cosmic ray spectrum has been measured from 10^8 to 10^{20} eV and it generally follows a power-law behavior. It has exhibited two prominent features known as the "knee" (at ∼3×10^{15} eV) and the "ankle" (at ∼3×10^{18} eV). Galactic cosmic rays are believed to be accelerated by supernova remnant shock fronts (SNR), though it is difficult to explain the acceleration up to the knee energy using this mechanism [18, 19]. The transition between the knee and the ankle, where the cosmic rays likely transit from their Galactic to their extragalactic origin, needs to be further understood. Accurate measurement of the mass composition in the knee region is crucial to resolve these issues, including determining the end of the Galactic cosmic ray spectrum. Furthermore, the absolute calibration of the energy and composition of cosmic rays up to ∼ 100 TeV by comparing it with direct measurements and by understanding the hadronic interaction models used for the interpretation of air shower data is very important in reducing systematic uncertainties.

Precision measurements by direct experiments, such as PAMELA [20], AMS-02 [21], DAMPE [22], and CALET [23], have discovered new features in the low-energy part of the cosmic ray spectrum. Spectral hardening around ∼ 500 GeV has been confirmed by multiple experiments. Spectral softening of around 10 TeV was first indicated by the CREAM experiment. Now, it has been confirmed by both DAMPE and CALET experiment. Although the origin of these new spectral features is not known at the moment, but clearly shows the cosmic ray spectrum cannot be described by a single power-law below the Knee energy as was believed.

The limited statistics collected by the direct experiments do not allow one to investigate cosmic rays beyond about 100 TeV. The energy range 10^{14}–10^{18} eV, which covers the knee and the Galactic-to-extragalactic transition region, is instead investigated by extensive ground-based air shower arrays such as KASCADE-Grande [24], GRAPES-3 [25, 26], Tibet AS_γ [8], ARGO-YBJ [27, 28], HAWC [29], IceCube/IceTop [30], and Tunka [31]. Other observatories or upgrades of existing ones, such as LHAASO [32], SWGO [33], TAIGA[34] and IceTop [35], the Telescope Array [36], and Pierre Auger Observatory [37, 38], will also contribute to these investigations.

4.2 Cosmic ray anisotropy

The cosmic ray arrival directions are known to be highly isotropic at all energies, yet a very small ($\sim 10^{-4}$ to 10^{-3}) anisotropy has been measured in the past two decades. The study of cosmic ray anisotropy could provide a better understanding of the spatial distribution of cosmic ray sources and magnetic field distributions [39]. Ground-based EAS experiments located in the Northern hemisphere such as Tibet-ASγ [40, 41], ARGO-YBJ [42], Milagro [43], HAWC [44], and in the Southern hemisphere such as IceCube [45] have observed large-scale structures with a dominant dipolar component in TeV-PeV energies. The anisotropy is seen as an excess within the right ascension of $30^\circ \leq \alpha \leq 120^\circ$ and a large deficit within $150^\circ \leq \alpha \leq 250^\circ$. The high statistical collection of events by these experiments allows them to observe such a tiny amplitude of the anisotropy. Furthermore, anisotropies have been observed at ultra high energies ($\sim 10^{18}$ eV) by the Pierre Auger Observatory [46]. At these energies, the interstellar magnetic field plays the least significant role in bending the cosmic rays.

In addition to large-scale anisotropy, small-scale anisotropy structures with angular width less than 60° were first reported by the Milagro experiment. It observed two excess regions, namely region A and B with an excess at the level of $\sim (6 \pm 0.9) \times 10^{-4}$ and $\sim (4 \pm 0.4) \times 10^{-4}$, respectively [47]. The ARGO-YBJ experiment also observed the same regions [48]. The HAWC experiment has also observed these structures [49].

5 The GRAPES-3 experiment

GRAPES-3 consists of two main detector systems as shown in the schematic in Fig. 1; (1) an array of 400 closely spaced plastic scintillator detectors of 1 m^2 area each, spread over an area of 25,000 m^2, and (2) a tracking muon detector consisting of 16 modules of 35 m^2 area each.

Each scintillator detector measures all charged particles in EAS. An EAS trigger is generated when at least ten detectors register signals above 0.5 particle equivalents. The array's trigger rate is approximately 35 per second. The photomultiplier signals from each scintillator detector are transmitted to the control room via coaxial cables, where they are digitized by an analog-to-digital converter (ADC) to estimate particle density. The signal's

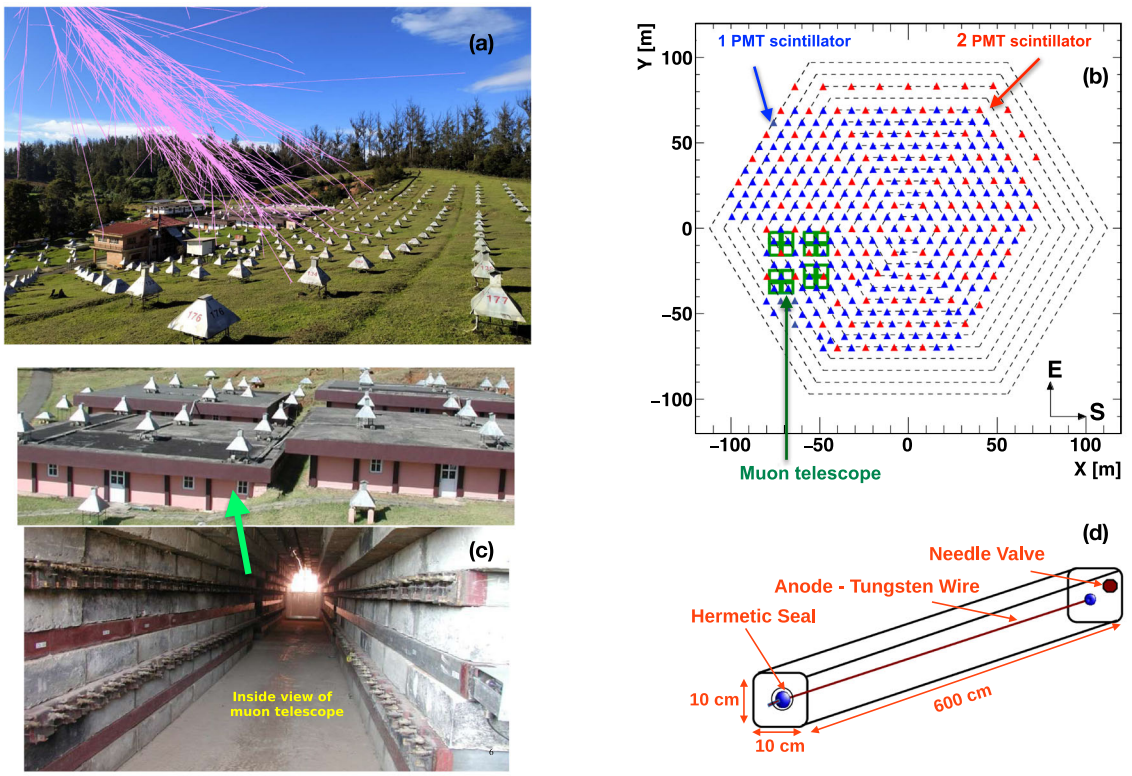

Fig. 1 **a** A view of the GRAPES-3 experiment with the scintillator detectors seen as white conical structure, **b** a schematic of the array, **c** four muon stations (top) and inside view of one of the muon detector stations (bottom), and **d** a schematic of the proportional counter

arrival time is digitized by a time-to-digital converter (TDC), which is used to estimate the shower's direction. The shower's core location, size, and age parameters are determined by fitting the lateral distribution of particle densities [50].

Each muon module consists of four layers of proportional counters (PRCs), with each PRC composed of square iron tubes that measure 6 m in length and have a cross section of 0.1m × 0.1m [51]. Muon tracking is based on hit information from two orthogonal layers of PRCs. A vertical muon threshold of 1 GeV is achieved due to the 550 g cm^{-2} of concrete shielding. When a shower trigger is received from the scintillator array, muon information is recorded. The muon component is crucial for determining the mass composition of primary cosmic rays and provides a means of distinguishing between gamma rays and charged cosmic rays. An independent data acquisition system records individual muons by detecting coincidences in all four PRC layers, measuring muon flux at ∼3000 counts per second per module, or around 50,000 per second across 16 modules.

5.1 Performances of the scintillator array

CORSIKA code was used to simulate cosmic rays in the atmosphere. In-house-developed code was used to perform the array simulation. Geant4 code was employed to determine the response of each scintillator detector. The performance of the scintillator array was evaluated through these simulations which is described in detail elsewhere [52]. The array is capable of triggering showers with energies as low as 1 TeV, largely due to the close spacing of the detectors. The median energy of the array was found to be 15 TeV. The trigger efficiency for five different primary masses is estimated from simulations. The array achieves over 90% trigger efficiency for proton-initiated showers at energies around 40 TeV for zenith angles below 18°. The same trigger efficiency for iron-initiated showers is reached at 80 TeV.

The core resolution for proton showers is 6 m at 40 TeV energy, which improves to 2 m at 100 TeV and ∼0.5 m at 1 PeV energy. The energy resolution is obtained by comparing the true energy with the reconstructed energy, and the energy bias is defined as the offset of the energy. It is about 65% at 40 TeV, which improves to 35% at 1 PeV. The energy bias is consistent with zero. The angular resolution of the array has improved significantly after correction for the curvature of the shower front based on size and age [50]. It was validated using observation of Moonshadow [53]. The angular resolution is 0.85° for all showers which improves to 0.35° at 100 TeV.

5.2 Results on cosmic ray proton spectrum

The cosmic ray proton spectrum from 50 TeV to 1.3 PeV was measured using data recorded by the GRAPES-3 experiment from 1 January 2014 to 26 October 2015. The details of the analysis and the results are provided in [54]. A total of 1.75×10^9 shower events were analyzed over a live time of approximately 460 days. After applying various selection criteria and cuts, 7.81×10^6 events remained. To ensure a trigger efficiency greater than 90%, only showers with a size larger than 10^4 were considered, corresponding to a primary proton energy of 50 TeV and 80 TeV for iron primaries. The showers were limited to a zenith angle of less than 18°.

The observed muon multiplicity distributions were compared with simulations assuming five primary mass compositions: proton (H), helium (He), nitrogen (N), aluminum (Al), and iron (Fe). Here, N represents the C–N–O group, Al represents the Mg–Al–Si group, and Fe represents the Mn–Fe–Co group. The relative contribution of each mass group was obtained using an unfolding technique, with particular focus on protons.

The proton size spectrum was derived from the data size spectrum using the composition weights, and the proton energy spectrum was obtained via unfolding. These results are presented in Fig. 2, alongside data from other direct

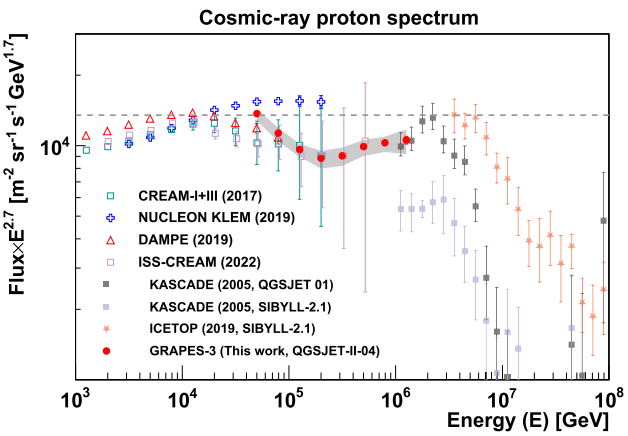

Fig. 2 Cosmic ray proton spectrum measured by the GRAPES-3 experiment from 50 TeV to 1.3 PeV which is presented along with the results from space-based and ground-based experiments

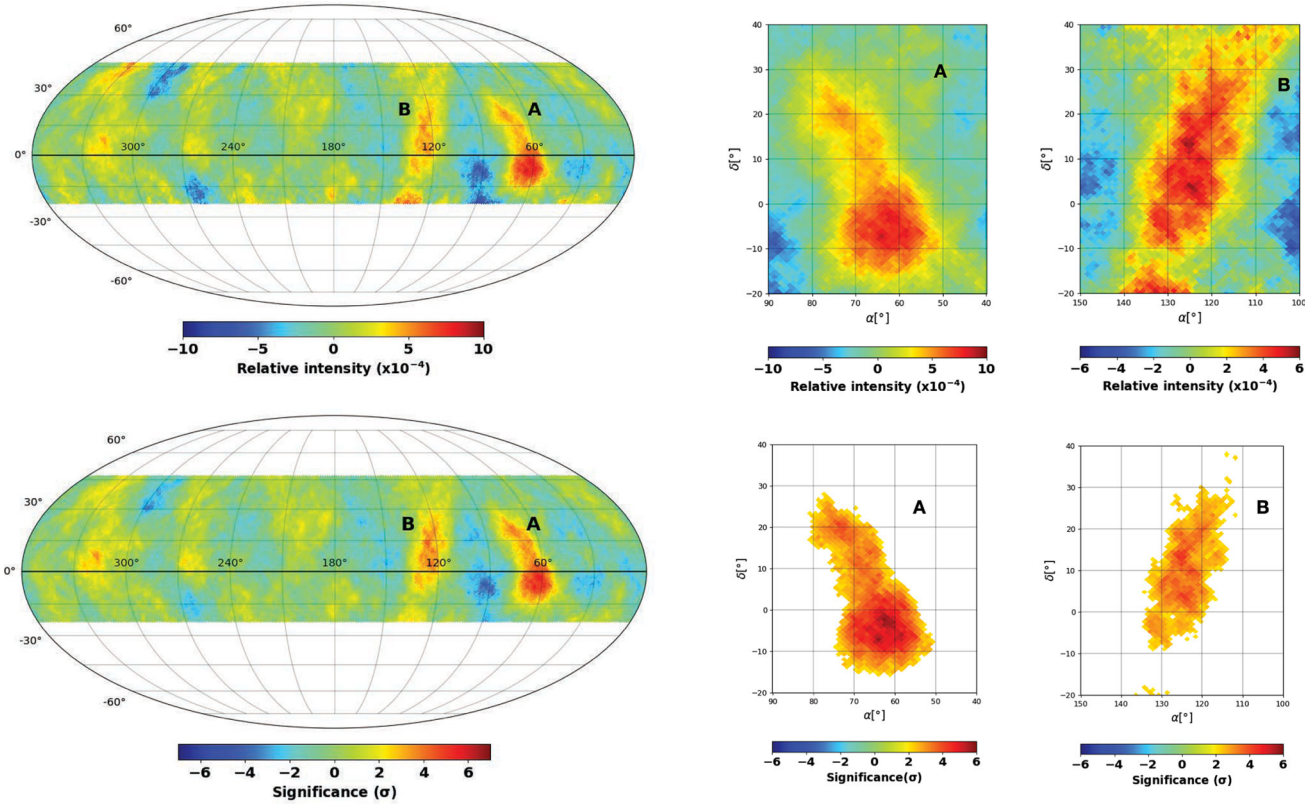

Fig. 3 Small-scale cosmic ray anisotropy observed by the GRAPES-3 experiment is shown including the relative intensity and significance maps. The two structures denoted by A and B are observed with significance of 6.8σ and 4.7σ, respectively

and indirect experiments. Statistical errors are smaller than the data point markers. The proton spectrum agrees well with direct measurements at lower energies and with the KASCADE spectrum obtained using the pre-LHC QGSJet01 hadronic model. A hardening of the spectrum is observed at 164±55 TeV, with spectral indices of -3.1 ± 0.19 and -2.59 ± 0.09 before and after the break point, respectively. These results indicate that the proton spectrum below the knee energy cannot be described by a single power-law model.

5.3 Results on cosmic ray anisotropy

Cosmic ray anisotropy was measured using shower events recorded by the GRAPES-3 scintillator array between 1 January 2014 and 31 December 2016, comprising 3.7×10^9 events. Detailed analysis and results are provided in [55]. The time scrambling method was used for the analysis. Two statistically significant structures, labeled A and B, were observed, as shown in Fig. 3. The amplitudes of regions A and B were measured to be $6.5\pm1.3)\times10^{-4}$ and $(4.9\pm1.4)\times10^{-4}$, respectively, with statistical significances of 6.8σ and 4.7σ. These results are consistent with observations from the Milagro, HAWC, and ARGO-YBJ experiments.

5.4 Upgrade of the GRAPES-3 experiment

The muon detector in the GRAPES-3 experiment plays a crucial role in measuring cosmic ray mass composition, conducting multi-TeV gamma-ray astronomy, and studying solar and atmospheric physics research. A new muon detector of an area similar to the existing one is currently under construction. Once completed, the expanded system will effectively double the muon detection area. Calculations indicate that this expanded detector will achieve the same sensitivity for gamma-ray detection in 1 year that the current detector would require 10 years to reach. Furthermore, it will enable more reliable mass separation of cosmic rays, particularly in the low-energy range (below 100 TeV).

The detector uses proportional counters (PRCs) (6 m×0.1m×0.1m) as its basic detection units. Almost 4,000 PRCs were successfully manufactured in the GRAPES-3 laboratory over a period of 3 years and have since been installed in the field. Front-end and FPGA-based DAQ electronics were also developed, with electronics installation

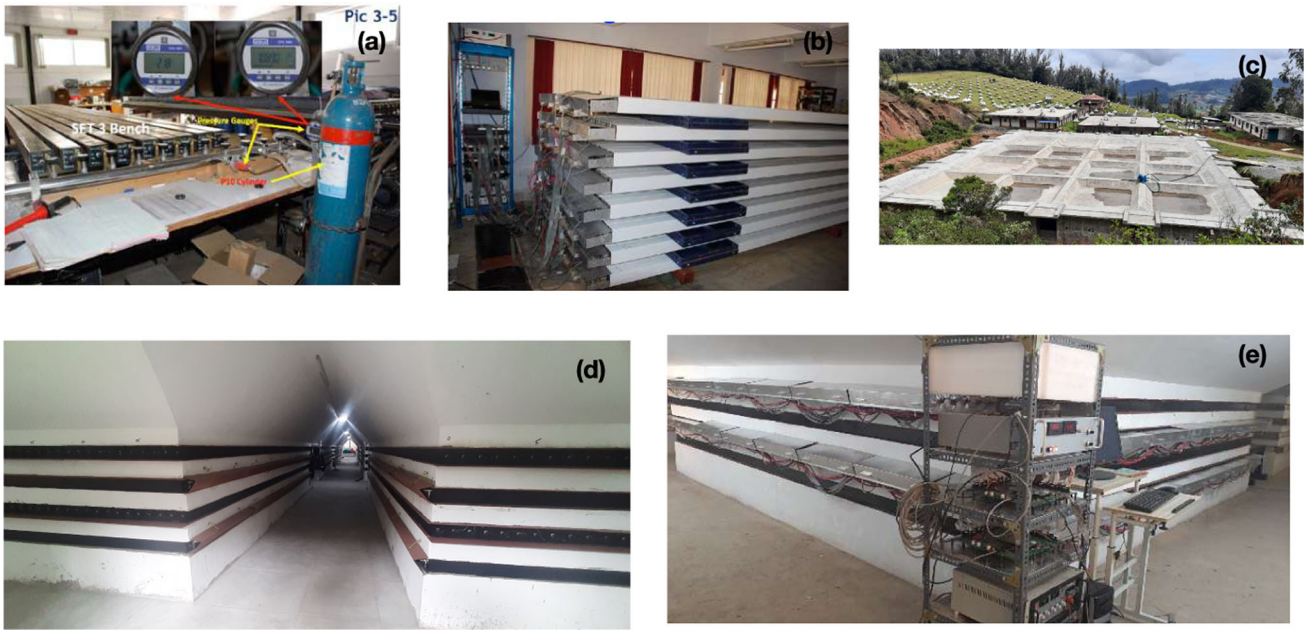

Fig. 4 **a** Test bench for PRC vacuum creation and gas filling, **b** testing of PRC performances, **c** top view of the new muon telescope, and **d** inside view of the new muon telescope, and **e** operation of the first module of the new muon telescope

currently in progress [56, 57]. The full operation of the new muon detector is expected within a year. The images of the new muon detector are shown in Fig. 4.

Funding Open access funding provided by Department of Atomic Energy.

References

1. R.L. Workman et al., (Particle Data Group). Progress Theor. Exp. Phys. **2022**, 083C01 (2022). https://doi.org/10.1093/ptep/ptac097
2. D. Venkatesan, B. Badruddin, Cosmic-ray intensity variations in the 3-dimensional heliosphere. Space Sci. Rev. **52**, 121–194 (1990). https://doi.org/10.1007/BF00704241
3. W. Baade, F. Zwicky, Cosmic rays from Super-Novae. Proc. Natl. Acad. Sci. **20**, 259–263 (1934). https://doi.org/10.1073/pnas.20.5.259
4. V.L. Ginzburg, S.I. Syrovatski, Origin of cosmic rays. Soviet Physics Uspekhi **9**, 223–235 (1966). https://doi.org/10.1070/PU1966v009n02ABEH002871
5. M. Aguilar et al., The Alpha Magnetic Spectrometer (AMS) on the international space station: Part II - Results from the first seven years. Phys. Rep. **894**, 1–116 (2021). https://doi.org/10.1016/j.physrep.2020.09.003
6. N. Cannady et al., Characteristics and Performance of the CALorimetric Electron Telescope (CALET) Calorimeter for Gamma-Ray Observations. Astrophys. J. Suppl. Ser. **238(16pp)**, 5 (2018). https://doi.org/10.3847/1538-4365/aad6a3
7. J. Chang et al., The DArk matter particle explorer mission. Astropart. Phys. **95**, 6–24 (2017). https://doi.org/10.1016/j.astropartphys.2017.08.005
8. M. Amenomori et al., Cosmic-ray energy spectrum around the knee obtained by the Tibet experiment and future prospects. Adv. Space Res. **47**, 629–639 (2011). https://doi.org/10.1016/j.asr.2010.08.029
9. Z. Chao et al., The Large High Altitude Air Shower Observatory (LHAASO) Science Book (2021 Edition), https://doi.org/10.48550/arXiv.1905.02773. arXiv:1905.02773v4

10. A.U. Abeysekara et al., The High-Altitude Water Cherenkov (HAWC) observatory in México: the primary detector. Instrum. Methods Phys. Res. A **1052**, 168253 (2023). https://doi.org/10.1016/j.nima.2023.168253Nuclear
11. S.K. Gupta et al., GRAPES-3-A high-density air shower array for studies on the structure in the cosmic-ray energy spectrum near the knee. Nucl. Instrum. Methods Phys. Res. A **540**, 311–323 (2005). https://doi.org/10.1016/j.nima.2004.11.025
12. P.K. Mohanty et al., Measurement of some EAS properties using new scintillator detectors developed for the GRAPES-3 experiment. Physics **31**, 24–36 (2009). https://doi.org/10.1016/j.astropartphys.2008.11.004Astroparticle
13. T. Antoni et al., The cosmic-ray experiment KASCADE. Nucl. Inst. Methods Phys. Res. A **513**, 490–510 (2003). https://doi.org/10.1016/S0168-9002(03)02076-X
14. W.D. Apel et al., The KASCADE-Grande experiment. Instruments and Methods in Physics Research A **620**, 202–216 (2010). https://doi.org/10.1016/j.nima.2010.03.147Nuclear
15. R. Abbasi et al., (IceCube Collaboration), IceTop: The surface component of IceCube. Nuclear Instrumentation and Methods in Physics Research A **700**, 188–220 (2013). https://doi.org/10.1016/j.nima.2012.10.067
16. A. Aab, The Pierre Auger Cosmic Ray Observatory. Instruments and Methods in Physics Research A **798**, 172–213 (2015). https://doi.org/10.1016/j.nima.2015.06.058Nuclear
17. T. Abu-Zayyad et al., The surface detector array of the Telescope Array experiment. Nuclear Instrumentation and Methods in Physics Research A **689**, 87–97 (2012). https://doi.org/10.1016/j.nima.2012.05.079
18. P. Blasi, The origin of galactic cosmic rays. Astron. Astrophys. Rev. **21**, 70 (2013). https://doi.org/10.1007/s00159-013-0070-7
19. A.R. Bell, Cosmic ray acceleration. Astropart. Phys. **43**, 56–70 (2013). https://doi.org/10.1016/j.astropartphys.2012.05.022
20. O. Adriani et al., PAMELA Measurements of Cosmic-Ray Proton and Helium Spectra. Science **332**, 69–72 (2011). https://doi.org/10.1126/science.1199172
21. M. Aguilar et al., Precision Measurement of the Proton Flux in Primary Cosmic Rays from Rigidity 1 GV to 1.8 TV with the Alpha Magnetic Spectrometer on the International Space Station. Phys. Rev. Lett. **114**, 171103 (2015). https://doi.org/10.1103/PhysRevLett.114.171103
22. DAMPE Collaboration, Q. An et al., Measurement of the cosmic ray proton spectrum from 40 GeV to 100 TeV with the DAMPE satellite. Science Advances **5**, eaax3793 (2019). https://doi.org/10.1126/sciadv.aax3793
23. O. Adriani et al., Direct Measurement of the Cosmic-Ray Proton Spectrum from 50 GeV to 10 TeV with the Calorimetric Electron Telescope on the International Space Station. Phys. Rev. Lett. **122**, 181102 (2019). https://doi.org/10.1103/PhysRevLett.122.181102
24. KASCADE-Grande Collaboration, W.D. Apel et al., Kneelike structure in the spectrum of the heavy component of cosmic rays observed with KASCADE-Grande. Physical Review Letters **107**, 171104 (2011). https://doi.org/10.1103/PhysRevLett.107.171103
25. H. Tanaka et al., Studies of the energy spectrum and composition of the primary cosmic rays at 100–1000 TeV from the GRAPES-3 experiment. J. of Phys. G: Nucl. Part. **39**, 025201 (2012). https://doi.org/10.1088/0954-3899/39/2/025201
26. F. Varsi et al., Cosmic ray energy spectrum and composition measurements from the GRAPES-3 experiment: Latest results. Proceedings of Science (ICRC2021) **395**, 388 (2021). https://inspirehep.net/files/363387bc9e92e9aebf774fbcc16b5bb3
27. B. Bartoli et al., Cosmic ray proton plus helium energy spectrum measured by the ARGO-YBJ experiment in the energy range 3–300 TeV. Physical Review D **91**, 112017 (2015). https://doi.org/10.1103/PhysRevD.91.112017
28. B. Bartoli et al., Knee of the cosmic hydrogen and helium spectrum below 1 PeV measured by ARGO-YBJ and a Cherenkov telescope of LHAASO. Physical Review D **92**, 092005 (2015). https://doi.org/10.1103/PhysRevD.92.092005
29. H.A.W.C. Collaboration, R. Alfaro et al., All-particle cosmic ray energy spectrum measured by the HAWC experiment from 10 to 500 TeV. Physical Review D **96**, 122001 (2017). https://doi.org/10.1103/PhysRevD.96.122001
30. M.G. Aartsen et al., Cosmic ray spectrum and composition from PeV to EeV using 3 years of data from IceTop and IceCube. Physical Review D **100**, 082002 (2019). https://doi.org/10.1103/PhysRevD.100.082002
31. N.M. Budnev et al., The primary cosmic-ray energy spectrum measured with the Tunka-133 array. Astropart. Phys. **117**, 102406 (2020). https://doi.org/10.1016/j.astropartphys.2019.102406
32. H. He for the LHAASO Collaboration, Design of the LHAASO detectors. Radiation Detector Technology and Methods **2**, 7 (2018). https://doi.org/10.1007/s41605-018-0037-3
33. H. Schoorlemmer for SWGO collaboration, A next-generation ground-based wide field-of-view gamma-ray observatory in the southern hemisphere. Proceedings of Science (ICRC2019) **358**, 785 (2019). https://pos.sissa.it/358/785/pdf
34. TAIGA Collaboration, N. Budnev et al., TAIGA the Tunka Advanced Instrument for cosmic ray physics and Gamma Astronomy - present status and perspectives. Journal of Instrumentation **9**, C09021 (2014). https://doi.org/10.1088/1748-0221/9/09/C09021
35. A. Haungs for the IceCube Collaboration, A Scintillator and Radio Enhancement of the IceCube Surface Detector Array. Web of Conferences **210**, 06009 (2019). https://doi.org/10.1051/epjconf/201921006009EPJ
36. S. Ogio for the Telescope Array Collaboration, Telescope Array Low energy Extension: TALE, JPS Conference Proceedings **19**, 011026 (2018). https://doi.org/10.7566/JPSCP.19.011026
37. D. Bergman et al., jNICHE: Prototype detectors of a non-imaging Cherenkov array at the TA site, Proceedings of Science (ICRC2017) **301**, 415 (2018). https://pos.sissa.it/301/415/

38. Pierre Auger Collaboration, A. Aab et al., The Pierre Auger Observatory Upgrade - Preliminary Design Report, https://arxiv.org/abs/1604.03637arXiv:1604.03637 [astro-ph.IM]
39. O. Deligny, Measurements and implications of cosmic ray anisotropies from TeV to trans-EeV energies. Physics **104**, 13–41 (2019). https://doi.org/10.1016/j.astropartphys.2018.08.005Astroparticle
40. M. Amenomori et al., Anisotropy and Corotation of Galactic Cosmic Rays. Science **314**, 439–443 (2006). https://doi.org/10.1126/science.1131702
41. M. Amenomori et al., Northern Sky Galactic Cosmic Ray Anisotropy between 10 and 1000 TeV with the Tibet Air Shower Array. Astrophys. J. **836**, 153 (2017). https://doi.org/10.3847/1538-4357/836/2/153
42. B. Bartoli et al., Galactic Cosmic-Ray Anisotropy in the Northern Hemisphere from the ARGO-YBJ Experiment during 2008–2012. Astrophys. J. **861**, 93 (2018). https://doi.org/10.3847/1538-4357/aac6cc
43. A.A. Abdo et al., The Large-Scale Cosmic Ray Anisotropy as Observed with MILAGRO. Astrophys. J. **698**, 2121–2130 (2009). https://doi.org/10.1088/0004-637X/698/2/2121
44. A.U. Abeysekara et al., All-sky Measurement of the Anisotropy of Cosmic Rays at 10 TeV and Mapping of the Local Interstellar Magnetic Field. Astrophys. J. **871**, 96 (2019). https://doi.org/10.3847/1538-4357/aaf5cc
45. M.G. Aartsen et al., Anisotropy in cosmic-ray arrival directions in the southern hemisphere based on six years of data from the IceCube detector. Astrophys. J. **826**, 220 (2016). https://doi.org/10.3847/0004-637X/826/2/220
46. A. Aab et al., Large-scale Cosmic-Ray Anisotropies above 4 EeV Measured by the Pierre Auger Observatory. Astrophys. J. **868**, 4 (2018). https://doi.org/10.3847/1538-4357/aae689
47. A.A. Abdo et al., Discovery of Localized Regions of Excess 10-TeV Cosmic Rays. Phys. Rev. Lett. **101**, 221101 (2008). https://doi.org/10.1103/PhysRevLett.101.221101
48. B. Bartoli et al., Medium scale anisotropy in the TeV cosmic ray flux observed by ARGO-YBJ. Physical Review D **88**, 082001 (2013). https://doi.org/10.1103/PhysRevD.88.082001
49. A.U. Abeysekara et al., Observation of Small-Scale Anisotropy in the Arrival Direction Distribution of TeV Cosmic Rays with HAWC. Astrophys. J. **796**, 108 (2014). https://doi.org/10.1088/0004-637X/796/2/108The
50. V.B. Jhansi et al., The angular resolution of GRAPES-3 EAS array after improved timing and shower front curvature correction based on age and size. J. Cosmol. Astropart. Phys. **07**, 024 (2020). https://doi.org/10.1088/1475-7516/2020/07/024
51. Y. Hayashi et al., A large area muon tracking detector for ultra-high energy cosmic ray astrophysics-the GRAPES-3 experiment. Nuclear Instrumentation Method in Physics Research A **545**, 643–657 (2005). https://doi.org/10.1016/j.nima.2005.02.020
52. P.K. Mohanty et al., Recent results from the GRAPES-3 experiment. Proceedings of Science (ICRC2023) **444**, 535 (2023). https://doi.org/10.22323/1.444.0535
53. D. Pattanaik et al., Validating the improved angular resolution of the GRAPES-3 air shower array by observing the Moon shadow in cosmic rays. Physical Review D **106**, 022009 (2022). https://doi.org/10.1103/PhysRevD.106.022009
54. F. Varsi et al., Evidence of a Hardening in the Cosmic Ray Proton Spectrum at around 166 TeV Observed by the GRAPES-3 Experiment. Phys. Rev. Lett. **132**, 051002 (2024). https://doi.org/10.1103/PhysRevLett.132.051002
55. M. Chakraborty et al., Small-scale cosmic ray anisotropy observed by the GRAPES-3 experiment at TeV energies. Astrophys. J. **961**, 87 (2024). https://doi.org/10.3847/1538-4357/ad132bThe
56. K. Ramesh et al., High-Performance and Low-Noise Front-End Electronics for GRAPES-3 Muon Telescope. Exp. Astron. **56**, 31–37 (2023). https://doi.org/10.1007/s10686-023-09898-5
57. A. Jain et al., An Advanced Triggerless Data Acquisition System for the GRAPES-3 Muon Detector. Proceedings of Science (ICRC2021) **395**, 257 (2021). https://doi.org/10.22323/1.395.0257